Single Mask, Large Force, and Large Displacement Electrostatic Linear Inchworm Motors

Richard Yeh, Seth Hollar, and Kristofer S. J. Pister

***Abstract*—We have demonstrated a family of large force and large displacement electrostatic linear inchworm motors that operate with moderate to high voltages. The inchworm motor design decouples actuator force from total travel and allows the use of electrostatic gap-closing actuators to achieve large force and large displacement while consuming low power. A typical inchworm motor measures 3 mm $\times$ 1 mm $\times$ 50 μm and can lift over 130 times its own weight. One motor has achieved a travel of 80 μm and a calculated force of 260 μN at 33 V. The force density of that motor was 87 μN/mm^2 at 33 V and the energy efficiency was estimated at 8%. Another motor displaced the shuttle at an average velocity of almost 4 mm/s and achieved an estimated power density of 190 W/m^3. Motors were cycled 23.6 million times for over 13.5 h without stiction. This family of motors is fabricated in silicon-on-insulator (SOI) wafers using a single mask. [663]**

***Index Terms*—Actuators , electrostatics, gap closing, inchworm motors, microrobots.**

I. Introduction

MEMS applications often require large force, large displacement, low-power, and energy-efficient actuators. One example would be autonomous microrobots which require hundreds of micronewtons of force, tens of microns of travel, and must power actuators and electronics from onboard energy sources [1]. However, most MEMS actuators either have a force-displacement tradeoff or simply have small displacements. In addition, many actuators, such as those based on thermal or magnetic principles, possess very low energy efficiency. Piezoelectric actuators can operate with higher energy efficiency at moderate voltages but are more difficult to fabricate and integrate with other silicon microrobot mechanisms. Electrostatic actuators are far more efficient than thermal or magnetic actuators and are easier to fabricate and integrate with other silicon mechanisms than piezoelectric actuators. In 1995, we demonstrated the first MEMS electrostatic linear inchworm motor [2]. This motor achieved moderate displacement by accumulating 2 μm displacements over time. These motors made use of electrostatic gap-closing actuators (GCA), which possess high force densities at small displacements, consume low power (tens of μW), and are energy-efficient.

Fig. 1 compares the estimated force-densities and travel of several published MEMS motors. Our first inchworm motor was fabricated in MUMPS which provides thin-film (1.5–2 μm) polysilicon. The process had an aspect ratio of 2 which limited the force density of the motor. In addition, the stress gradient inherent in LPCVD polysilicon films limited the overall size of the motors. In 1997, Baltzer *et al.* [3] reported a GCA inchworm motor fabricated in a similar process and improved on total travel. Saif *et al.* [4] demonstrated the potential for a large-force electrostatic actuator with a high aspect-ratio millimeter-sized comb-drive actuator which produced 4.5 mN in 20 mm^2 but with limited travel ($<$15 μm). The Sandia Microengine [5] used a low aspect ratio comb-drive actuator which had low force density but achieves large travel and large torque using gear trains. In addition, the engine can produce high power due to the high resonant frequency of the comb-drives.

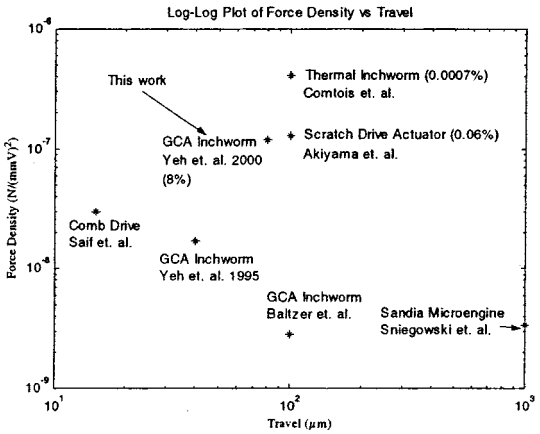

Fig. 1. log–log plot of the force densities normalized to the voltage squared versus the stroke of several motors [2]–[6]. Energy efficiency in parenthesis.

The motors presented in this paper are fabricated in silicon-on-insulator (SOI) wafers with an anisotropic etch aspect ratio of up to 25 : 1. This enables us to achieve a theoretical force density of approximately 1 mN/mm^2 at 30 V. Other MEMS motors with similar force densities are the thermal inchworm motors [6] and the scratch drive actuators [7]. However, thermal actuators suffer from tremendous heat loss, and scratch drive actuators require a large amount of force to transform vertical mechanical work into lateral mechanical work. Both of these motors are extremely inefficient and thus would not be appropriate for most autonomous applications.

II. Fabrication

The inchworm motors were fabricated by the following process (see Fig. 2). We start with an SOI wafer that has a silicon device layer thickness of 15–50 μm, a buried oxide layer thickness of 2 μm, and a silicon handle wafer. A 0.5 μm-thick oxide masking layer is thermally grown on the wafer. The oxide masking layer is patterned (only mask) and then the photoresist

Manuscript received February 16, 2001; revised February 3, 2002. Subject Editor O. Tabata.

The authors are with the Berkeley Sensor and Actuator Center, Department of Electrical Engineering and Computer Science, University of California, Berkeley, CA 94720 USA.

Publisher Item Identifier 10.1109/JMEMS.2002.800937.

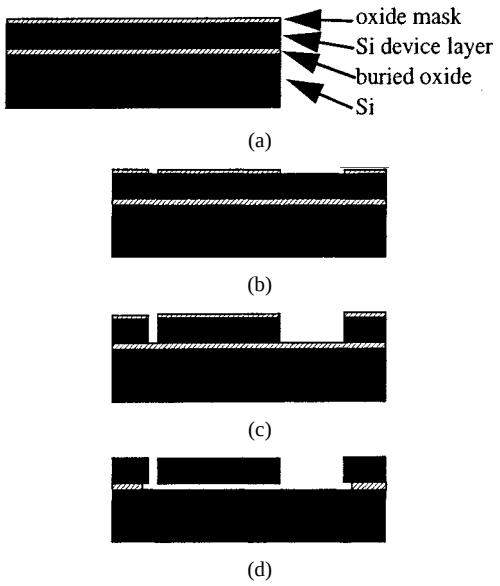

Fig. 2. Single-mask fabrication process. (a) Oxidize SOI wafer to create mask layer. (b) Pattern oxide mask. (c) Etch Si device layer. (d) HF etch of buried oxide.

(PR) is removed to prevent PR from being hardened in the silicon etch. The exposed silicon areas are etched down to the buried oxide using the Bosch deep silicon etching process. The wafer is diced and then the sacrificial oxide layer is removed in a timed etch that allows narrow structures to be released while wide structures are anchored by the un-etched oxide underneath. To reduce release stiction, the wafer is dried in a critical point dryer. After mounting the chip to a package, wires are bonded directly to bare silicon pads on the chip to actuate the motors.

III. Theory of Operation

The inchworm motor consists of two clutch-drive actuators and a sliding shuttle (see Fig. 3). Each actuator is composed of an array of GCAs (gap-closing actuators) for actuation and a set of flexural springs for restoring forces. To move the shuttle, the clutch engages the shuttle using the clutch-GCA array and then pulls the shuttle forward using the drive-GCA array.

An SEM micrograph of one of the inchworm motors fabricated is shown in Fig. 4. Like Fig. 3, Fig. 4(a) shows a pair of clutch-drive actuators. In the close-up [Fig. 4(b)], the drive-GCA array is composed of an array of horizontal silicon fingers, and the clutch-GCA array vertical silicon fingers. Fig. 4(d) shows a simplified drawing of the fabricated motor. The movable frame of the motor is marked as "released structures" and is electrically attached to the "ground anchor" via the parallel flexural springs. The SOI sections marked "anchor" are anchored to the substrate via the buried oxide and are the locations where wires are directly bonded. Applying voltages to "drive anchor" and "clutch anchor" actuates the drive and clutch GCA arrays, respectively.

During the inchworm cycle, the two clutch-drive actuators alternately move the shuttle to accumulate large displacements, which eliminates the force-displacement tradeoff inherent in electrostatic gap-closing actuators. A complete cycle is accomplished in four steps (see Fig. 5): (a) clutch A engages shuttle

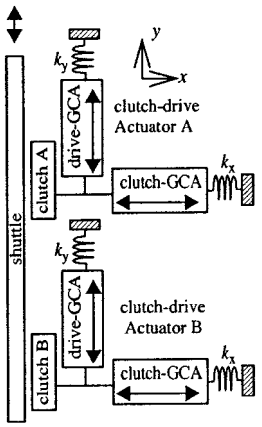

Fig. 3. Diagram of a linear inchworm motor.

(b) clutch B disengages while drive B pulls shuttle forward. (c) clutch B engages shuttle and (d) clutch A disengages while drive B pulls shuttle forward. The cycles are repeated as necessary. Steps (a) and (c) move the shuttle forward, so that in a complete cycle the sum of the two steps must be equivalent to the pitch of the gear teeth (see Section VI). As apparent in Fig. 5, the parallel flexural beams guide the movement of the clutch in a strictly linear direction. The resolution of the displacement is defined and limited by the lithography and aspect ratio of the fabrication process.

IV. Actuator Design

The gap-closing actuator consists of two parallel beams of length, l, and thickness, t. The beams are separated by a gap, g_1. One beam is anchored to the substrate while the other is supported by a spring. When a voltage is applied between the two beams, an electric field in the gap causes the spring-supported beam to move toward the stationary beam. An anchored gap-stop biased at the same potential prevents shorting between the two beams. The gap between the gap-stop and the GCA beam, g_3, is less than the gap between the GCA beams, g_1. This gap, g_3, defines the travel of the GCA. To generate more force, an array of parallel GCAs is used in the motor. Fig. 6 shows the diagram of an array of two GCAs separated by a gap of, g_2.

V. Analysis

Now we can examine the one dimensional dynamic analysis of the moving GCA array. We consider the following forces in our model:

$$m\ddot{x} = F_{e1} + F_{e2} + F_s + F_{sq} + F_L \tag{1}$$

where F_{e1}, F_{e2} are the electrostatic forces acting from the left and right sides of the beam (see Fig. 6), respectively, F_s, is the spring restoring force, and F_{sq} is the squeeze film damping forces again, acting from the left and right sides, respectively. F_L is the load. The electrostatic force, F_{e1}, between the two beams in a GCA is given by

$$F_{e1} = \frac{1}{2}\varepsilon_o N V_{app}^2 \frac{tl}{(g_1 - x)^2} = \frac{k_e}{(g_1 - x)^2} \tag{2}$$

where g_1 is the initial gap distance between the two GCA beams, V_{app} is the applied potential across the two beams, t is the thick-

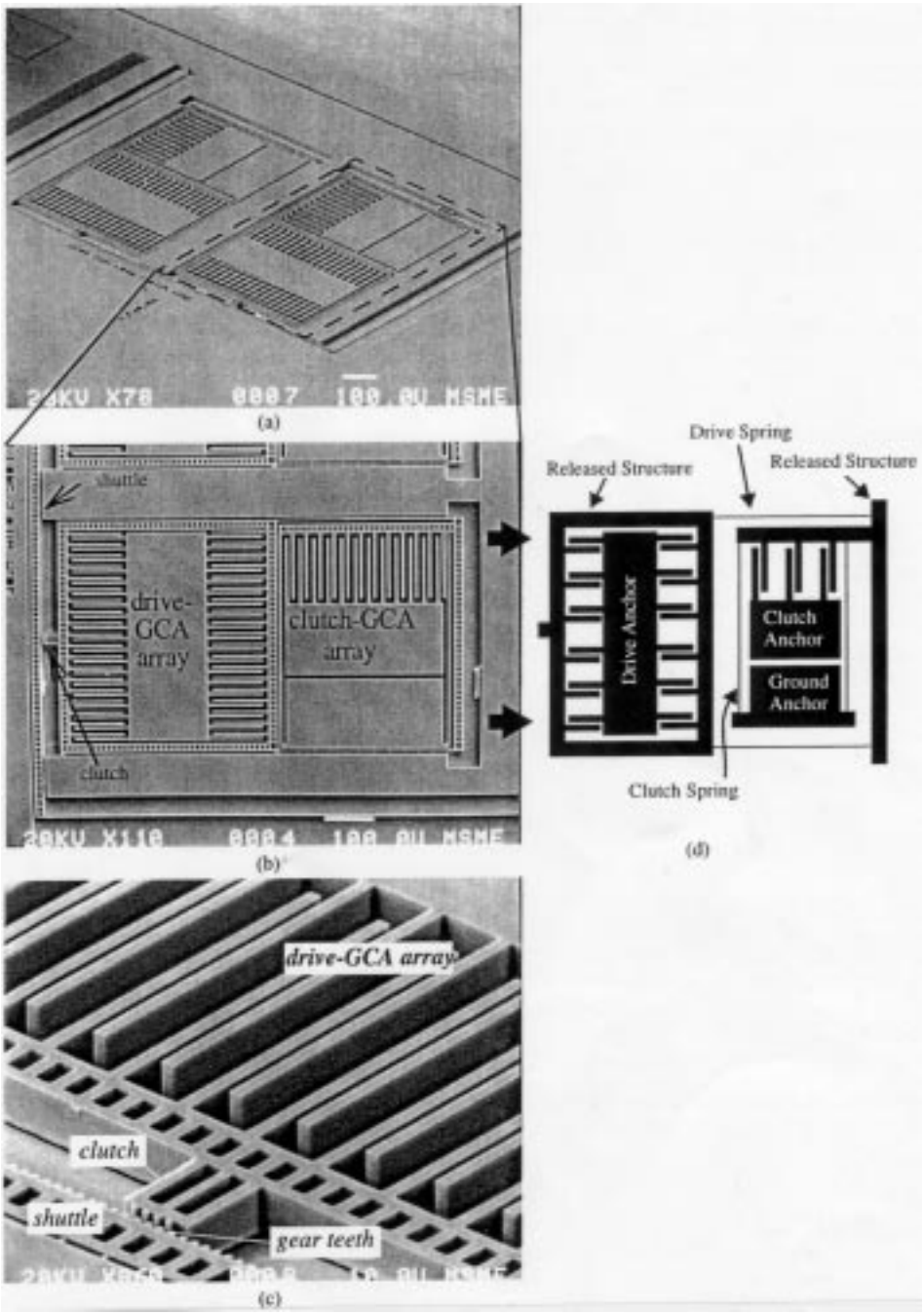

Fig. 4. (a) SEM of an inchworm motor fabricated on an SOI wafer. This motor displaced the shuttle by 48 μm in 12 cycles. The displacement was limited only by this particular shuttle design (not force-limited). (b) SEM close-up of the x–y actuator and clutch. Note the arrays of gap-closing actuators. (c) SEM close-up of the clutch-GCA array, clutch, and shuttle. (d) A simplified drawing of (b) showing the anchored and released structures of the clutch-drive actuator.

ness of the beam, l is the overlapping length of the beams, ε_o is the permittivity of air, N is the number of GCAs in the array, and x is the position of the moving beam. Likewise, the parasitic electrostatic force, F_{e2}, between the moving beam of one GCA and the stationary beam of the next GCA has a similar equation. To maximize the force density of the GCA array, g_2 is calculated to be approximately 2.8 larger than g_1. The restoring force of the support springs for the moving beams is given by Hooke's Law. The fourth force in our model is due to squeeze film damping. The force becomes significant when the gap between the beams become small compared to the length and thickness of the beams. The following damping force equation is based on Starr [8]:

$$F_{sq} = \frac{N\left(1 - 0.6\,\frac{t}{l}\right) t^3 l \mu}{(g_1 - x)^3}\,\dot{x} = \frac{-b\dot{x}}{(g_1 - x)^3} \tag{3}$$

where μ is the viscosity of air and $t < l$. Substituting (2) and (3) into (1), we have the 1-D dynamics equation for the supported beam:

$$m\ddot{x} + \frac{b\dot{x}}{(g_1 - x)^3} + k_s x = k_e\left(\frac{1}{(g_1 - x)^2} - \frac{1}{(g_2 - x)^2}\right) + F_L. \tag{4}$$

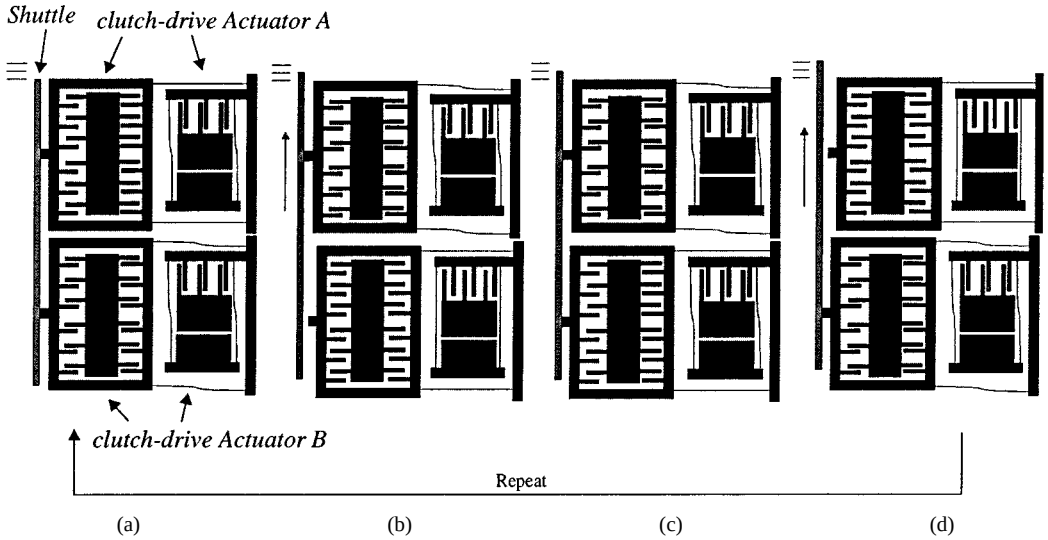

Fig. 5. Diagram of an inchworm cycle. (a) Clutch A engages shuttle. (b) Clutch B disengages shuttle and drive A pulls shuttle forward. (c) Clutch B engages shuttle. (d) Clutch A disengages shuttle and drive B pulls shuttle forward. Cycle is then repeated.

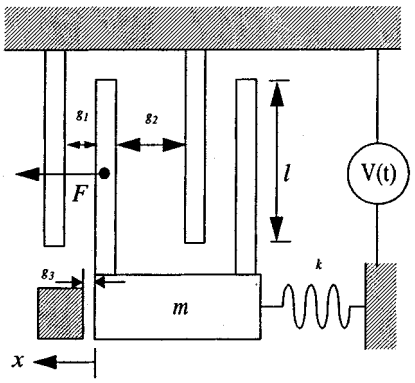

Fig. 6. Diagram of an array of two gap-closing actuators.

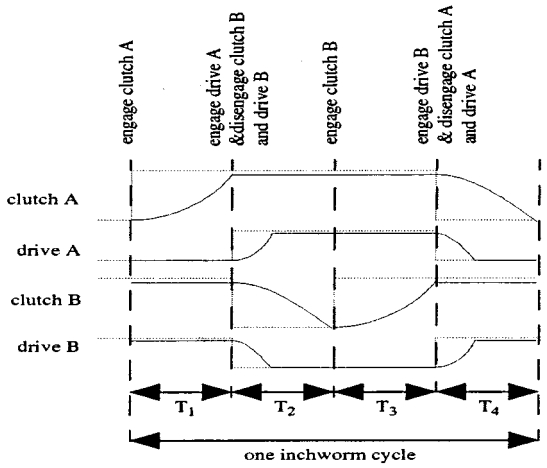

Fig. 7. Timing diagram for the inchworm motor through one cycle as depicted by Fig. 5. The dotted lines indicate the drive signals and the solid lines indicate simulated responses of the beam positions.

Below is the pull-in voltage, V_{pi}, which is the *minimum* voltage required to close the gap with no external load:

$$V_{pi} = \sqrt{\frac{8}{27}\frac{k_s g_1^3}{\varepsilon t^3 l N}}\,. \tag{5}$$

A. Speed

The maximum frequency of operation for the GCA inchworm motors is limited by the time it takes to close (pull-in) and open (pull-out) the gap. (4) can be solved numerically for the position, $x(t)$. Fig. 7 shows the state of one of our motors through one inchworm cycle as predicted by the model. The cycle time is equal to the summation of T_1 to T_4. Since the two clutch-drive actuators are identical, T_1 equals T_3 and T_2 equals T_4. The minimum cycle time is equal to

$$T = 2(T_1 + T_2). \tag{6}$$

The minimum of T_1 is limited by the pull-in time of clutch A and the minimum of T_2 is limited by the maximum of the pull-in time of drive A, pull-out time of clutch B, and pull-out time of drive B. According to the model, the pull-in time can be decreased by increasing the applied voltage as it is proportional to $1/V^2$ and the pull-out time can be decreased by increasing the spring constant as it is proportional to $\sqrt{1/k}$. For this model, we assumed that any bouncing from impacts of the clutch to the shuttle and released structure (moving GCA beams) to the gap stops was negligible compared to the other time constants of the system.

B. Scaling Effects

The effect as all dimensions, λ, are scaled down isotropically is shown in Table I. Details are described in [10]. The power density scales favorably as the minimum feature size decreases.

The only nonintuitive scaling effect above is in the electrostatic force which scales as λ^2. This is because catastrophic pull-in and shorting of GCA beams forces voltage-scaling as a fixed design geometry is scaled [11]. Above this maximum V_{pi}, the GCA beams will pull in toward each other due to electrostatic attraction and short out.

TABLE I

Unit	Scaling
Electrostatic Force	λ^2
Natural Frequency	$1/\lambda$
Squeeze film damping force	λ
Power Density	$1/\lambda$

C. Power

The power model of the inchworm motor can be described similarly to power dissipation of an IC digital circuit. The motor operates by closing and opening GCAs periodically at some defined frequency, f. Alternatively, we can think of the motor as charging and discharging the capacitors that make up the GCA. For inchworm motors that operate with the same clutch and drive voltage, the power dissipated by the inchworm motor is described by:

$$P = C_{\text{tot}} V^2 \cdot f \tag{7}$$

where C_{tot} is the total capacitance of the motor:

$$C_{\text{tot}} = 2C_{\text{drive}} + 2C_{\text{clutch}} + C_{\text{parasitics}} \tag{8}$$

C_{drive} is the maximum capacitance of one of the drive actuators, and C_{clutch} is the maximum capacitance of one of the clutch actuators. Because the capacitance of the drive and clutch actuators increases as the gap between the fingers reduces, the energy consumed is measured at the point where there is maximum capacitance, namely when the fingers are closest together. The only capacitance to produce work on the load is C_{drive}. Therefore, to reduce power dissipation and to increase the power efficiency, C_{clutch} and $C_{\text{parasitics}}$ need to be minimized. C_{clutch} is directly proportional to the clutch-GCA array size which can be reduced by minimizing the force which engages the clutch to the shuttle. The clutch force required can be minimized by reducing the width of the beams supporting the clutch-GCA array (reducing V_{pi}) and adding gear teeth on the clutch and shuttle. However, there is a tradeoff between efficiency and speed. As mentioned in Section V, reducing the spring constant of the beams increases the time of pull-out, ultimately reducing the speed at which the motor can be operated. The source of $C_{\text{parasitics}}$ is between the bond pads and the substrate. To reduce $C_{\text{parasitics}}$, we use SOI wafers with the thickest buried oxide layer available ($\sim$2 μm) and minimize the bond pad and anchor areas.

As an example of motor efficiency, consider the following: To produce 1.5 mN of force using a 30-V supply and a 3-μm initial gap in the GCAs, an initial GCA capacitance of 10 pF is needed. If the final gap is one third of the initial gap, then the final GCA capacitance will be three times the initial capacitance. If we operate the GCA at 1 kHz, then the power dissipated in the clutch-drive actuator would be 27 μW while producing 3 μW of power for an efficiency of 11%.

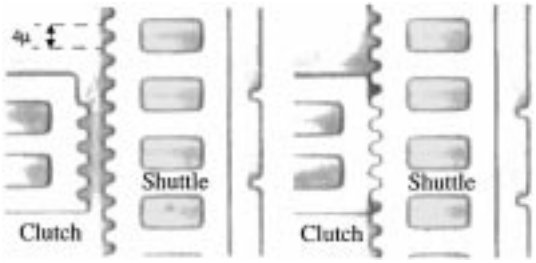

(a) (b)

Fig. 8. Close-up of gear teeth. In (a) clutch is not engaged to shuttle and in (b) clutch is engaged. Gear teeth were drawn 2.8 μm wide. Lateral etching of gear teeth reduced width to $\sim$2 μm.

VI. Gear Teeth Consideration

As seen in Fig. 8, gear teeth are used to transfer the drive force from the actuators to the shuttle. The gear teeth reduce slippage between the clutch and shuttle when the engaged clutch is pulled by the drive actuators. Previous attempts that did not employ gear teeth resulted in slippage and ultimately reduced the total force possible by the motor. The gear teeth of the fabricated motors have a 4-μm pitch allowing for 2 μm of travel per activation of the drive GCAs. The teeth are drawn in CAD with a 2.8-μm width. Because of the 25 : 1 vertical to lateral selectivity of the Bosch process silicon etch, the final tooth width is reduced to $\sim$2 μm. Should the teeth be too wide, the clutch would not fully engage the shuttle, increasing the chance of slippage. Some tolerance is given when undersizing the gear teeth because the lateral etch increases g_3 (see Fig. 6), the step size of the motor. The increased step size compensates for the additional slop in the gear teeth.

Because each drive actuator moves the shuttle by half the pitch of the gears, the design requires that the two clutches in the motor be half a period apart from one another relative to the shuttle's teeth. Namely, once the clutch-drive actuator A engages and drives the shuttle forward by 2 μm, clutch B must have its teeth aligned with the shuttle for the next engagement.

VII. Results

Using a single mask to define the motors, we have fabricated and tested several versions of the inchworm motor. The etch was done with a commercial deep trench etcher with an aspect ratio of 25 : 1. As mentioned earlier, an SEM micrograph of one of the inchworm motors fabricated is shown in Fig. 4. The motor dimension is 1.5 mm $\times$ 1 mm $\times$ 15 μm on a silicon handle wafer. A similar motor with a travel of 52 μm was operated at a maximum frequency of 1 kHz, moving the shuttle by an average velocity of 4 mm/s. The theoretical frequency limit according to our model is 1.4 kHz. Experimentally, we measured the minimum timing T_1 as 0.16 ms and T_2 as 0.35 ms. Our theoretical results predict 0.17 ms and 0.18 ms for T_1 and T_2, respectively. While the data matches well for T_1, T_2 differs by about a factor of two. Possible reasons for extended cycle period could include extra time to disengage from the shuttle and actuator bouncing against gap stops. At this frequency, the power density of this motor is estimated at 190 W/m^3. At higher speeds, some slipping between the clutch and the shuttle was observed.

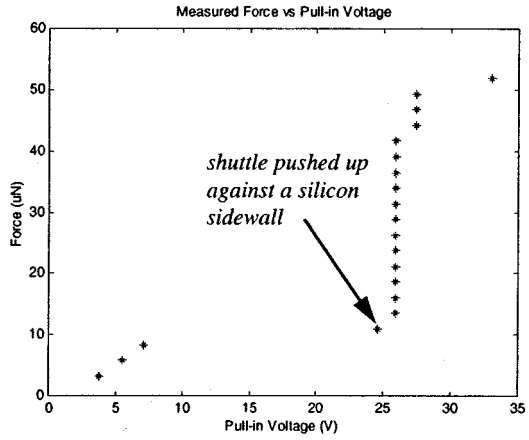

Fig. 9. Measured force versus pull-in voltage as the shuttle is displaced by 80 μm in 2 μm increments. The discontinuity occurred when the shuttle was pushed laterally against a silicon sidewall by the clutch-GCA.

Another version of the motor with dimensions of 1.5 mm $\times$ 2 mm $\times$ 50 μm on a silicon substrate was demonstrated with a travel of 80 μm and exerted a measured force of over 50 μN in excess of the friction it overcame. The force was measured by the displacement of the shuttle supporting springs. Fig. 9 shows the measured force versus V_{pi} as the shuttle is displaced by 80 μm in 2 μm step sizes. During operation, the shuttle was displaced laterally by the force of the clutch and subsequently pushed against the silicon sidewall on the other side of the shuttle [Fig. 4(c)]. The drive-GCA was nevertheless able to overcome the sidewall friction and pull the shuttle forward. The force generated, estimated by the V_{pi} required to displace the shuttle to 80 μm was 260 μN at 33 V. The force density achieved is 87 μN/mm^2. The theoretical upper limit of the force density at 33 V and an aspect ratio of 25 : 1 is approximately 1 mN/mm^2. This implies our motors have a fill factor of around 11% as the rest of the area is occupied by support structures, bonding pads, etc. Motors were operated for over 13.5 hours for a total of 23.6 million cycles without stiction.

VIII. Summary and Discussion

Electrostatic gap-closing actuators provide respectable force densities. These densities improve as lithographic limits decrease and anisotropic etch aspect ratios increase. GCAs are also limited in travel, so their large forces can only be applied over short distances. Fortunately, one GCA can be used to drive a clutch, allowing a second GCA to make intermittent contact with a moving shuttle. Repeated cycling through the gripping/pulling/releasing sequence generates large displacements while maintaining the full force available from the GCA primary using an inchworm-like motion.

Early problems with the electrostatic inchworm motors were related to clutch slipping, and clutch and gap-stop adhesion. The former problem has been addressed by using a gear teeth on the shuttle and clutch, and the latter by using a thicker SOI rather than thinner polysilicon structural layer. It is not clear why the adhesion problems have disappeared in the thicker single crystal silicon. The surface roughness of the sidewalls due to a DRIE etch may decrease the adhesion force, or the adhesion force may be relatively independent of film thickness, while the restoring force due to the support springs increases linearly with thickness.

The motors presented here are based on 2 μm lithography, with most features 3 μm or larger. Based on a simple dynamic model, it appears that these designs could be directly scaled down by a factor of 3 without a decrease in actuation voltage, and without seeing serious squeeze-film damping effects. Such a scaled motor would have the same force output, and the same velocity (smaller, faster steps), but only one tenth the layout area. Deep sub-micron scaling with this exact design will necessitate voltage scaling, but a careful mechanical re-design should enable motors that are ultimately limited by field emission from the GCAs, rather than destructive pull-in. We have demonstrated motors with 80 μm of motion, stepping rates of 1000 full steps/s corresponding to 4 mm/s shuttle velocity, and hundreds of μN of force. In all cases, displacement was limited by contact with a physical constraint (spring travel limits, nearby structures, etc.) rather than an intrinsic limit.

For microrobot applications, the energy efficiency of these motors is very attractive. While the 8% efficiency demonstrated is workable, the practical limits of an inductively charged, constant-charge GCA with similar mechanical power output should be closer to 80%. In addition, one of the motors with dimensions of 3 mm $\times$ 1 mm $\times$ 50 μm has demonstrated that it can lift over 130 times its own weight with 33 V. The inchworm motion of the motors with near-zero static power consumption is also attractive for solar powered microrobots of the future, which may need to integrate charge for many milliseconds before each phase of motor actuation.

References

[1] R. Yeh, E. Kruglick, and K. S. J. Pister, "Surface-micromachined components for articulated microrobots," *J. Microelectromechan. Syst.*, vol. 5, pp. 10–17, Mar. 1996.

[2] ——, "Microelectromechanical components for articulated microrobots," in *Proc. Eighth International Conference on Sensors and Actuators (Transducers '95)*, Stockholm, Sweden, June 25–29, 1995, pp. 346–349.

[3] M. Baltzer, T. Kraus, and E. Obermeier, "A linear stepping actuator in surface micromachining technology for low voltages and large displacements," in *Proc. Transducers' 97*, vol. 2, pp. 781–784.

[4] M. T. A. Saif and N. MacDonald, "A millinewton microloading device," in *Proc. Transducers' 95*, vol. 2, pp. 60–63.

[5] E. J. Garcia and J. J. Sniegowski, "Surface micromachined microengine," *Sens. Actuators, Phys. A*, vol. A48, no. 3, pp. 203–214.

[6] J. Comtois and V. Bright, "Applications for surface-micromachined polysilicon thermal actuators and arrays," *Sens. Actuators Phys. A*, vol. A58, no. 1, pp. 19–25.

[7] T. Akiyama and H. Fujita, "A quantitative analysis of scratch drive actuator using buckling motion," in *Proc. MEMS '95*, pp. 310–315.

[8] J. B. Starr, "Squeeze-film damping in solid-state accelerometers," in *IEEE Proc. Solid State Sensor and Actuator Workshop*, Hilton Head, SC, June 4–7, 1990, pp. 44–47.

[9] P. B. Chu and K. S. J. Pister, "Analysis of closed-loop control of parallel-plate electrostatic microgrippers," in *Proc. IEEE Int. Conf. on Robotics and Automation*, vol. 1, San Diego, CA, May 8–13, 1994, pp. 820–825.

[10] R. Yeh and K. S. J. Pister, "Design of low-power articulated microrobots," in *Proc. Int. Conference on Robotics and Automation, Workshop on Mobile Micro-Robots*, San Francisco, CA, April 23–28, 2000, pp. 21–28.

[11] P. M. Osterberg and S. D. Senturia, "M-test: A test chip for MEMS material property measurement using electrostatically actuated test structures," *J. Microelectromechan. Syst.*, vol. 6, no. 2, pp. 107–118, June 1997.

[12] B. Atwood, B. Warneke, and K. S. J. Pister, "Preliminary circuits for smart dust," in *Proc. IEEE 2000 Southwest Symposium on Mixed-Signal Design*, San Diego, CA, Feb. 27–29, 2000, pp. 87–92.

Richard Yeh received the B.S. degree in electrical engineering and computer science from the University of California at Berkeley in 1993, the M.S. degree in electrical engineering from the University of California at Los Angeles in 1995, and the Ph.D. degree in electrical engineering and computer science from the University of California at Berkeley in 2001.

Currently, working in the MEMS industry, his research interests include microrobotics, microactuation, microphotonics, packaging, and microfabrication techniques.

Seth Hollar received the B.S. degree in electrical engineering from Massachusetts Institute of Technology (MIT), Cambridge, in 1996, the M.S. degree in mechanical engineering from the University of California at Berkeley in 2000, and is currently pursuing the Ph.D. degree in mechanical engineering at the same.

For the last few years, he has been trying to make silicon walk.

Kristofer S. J. Pister received the B.A. degree in applied physics from the University of California at San Diego in 1982 and the M.S. and Ph.D. degrees in electrical engineering from the University of California at Berkeley in 1989 and 1992, respectively.

From 1992 to 1997, he was an Assistant Professor of Electrical Engineering at the University of California at Los Angeles. He is now a Professor of Electrical Engineering and Computer Sciences at the University of California at Berkeley. Since 1989, he has been trying (unsuccessfully) to make microrobots.

Dr. Pister is a Member of the DARPA ISAT and JASON groups, and the Defense Science Study Group.